

Open3DBench: Open-Source Benchmark for 3D-IC Backend Implementation and PPA Evaluation

Yunqi Shi^{1,2*}, Chengrui Gao^{1,2*}, Wanqi Ren^{1,2}, Siyuan Xu³, Ke Xue^{1,2}, Mingxuan Yuan³,
Chao Qian^{1,2†}, Zhi-Hua Zhou^{1,2}

¹National Key Laboratory for Novel Software Technology, Nanjing University, China

²School of Artificial Intelligence, Nanjing University, China

³Huawei Noah's Ark Lab, China

Abstract—This work introduces Open3DBench, an open-source 3D-IC backend implementation benchmark built upon the OpenROAD-flow-scripts framework, enabling comprehensive evaluation of power, performance, area, and thermal metrics. Our proposed flow supports modular integration of 3D partitioning, placement, 3D routing, RC extraction, and thermal simulation, aligning with advanced 3D flows that rely on commercial tools and in-house scripts. We present two foundational 3D placement algorithms: Open3D-Tiling, which emphasizes regular macro placement, and Open3D-DMP, which enhances wirelength optimization through cross-die co-placement with analytical placer DREAMPlace. Experimental results show significant improvements in area (51.19%), wirelength (24.06%), timing (30.84%), and power (5.72%) compared to 2D flows. The results also highlight that better wirelength does not necessarily lead to PPA gain, emphasizing the need of developing PPA-driven methods. Open3DBench offers a standardized, reproducible platform for evaluating 3D EDA methods, effectively bridging the gap between open-source tools and commercial solutions in 3D-IC design.

Index Terms—3D-IC, back-end implementation, PPA evaluation, open-source, OpenROAD.

I. INTRODUCTION

As process technology approaches its physical limits, advancing beyond sub-3nm nodes presents significant challenges. These include rising costs driven by extreme ultraviolet (EUV) lithography, increased design complexity, and reduced manufacturing yields [37]. To sustain Moore's Law [22], 2.5D and 3D integrated circuits (ICs), which enable higher-density integration along the z-axis, have emerged as promising alternatives. In addition to increasing the integration density and reducing the die area, the vertical interconnections in 3D-ICs also significantly shorten the wirelength, alleviate routing congestion, and improve timing performance.

To enable efficient 3D integration, advanced 3D stacking technologies have been extensively studied. Representative schemes include through-silicon vias (TSVs), micro-bumps, hybrid bonding terminals (HBTs), and monolithic interior vias (MIVs). Fig. 1 illustrates three typical 3D stacking methods. TSVs, with their large footprint, are increasingly being phased out due to their inability to meet high-density inter-die connection demands [37]. Micro-bumps, while smaller than TSVs, face scaling challenges below 10 μm , including reduced electrical performance, insufficient joint gaps, and the

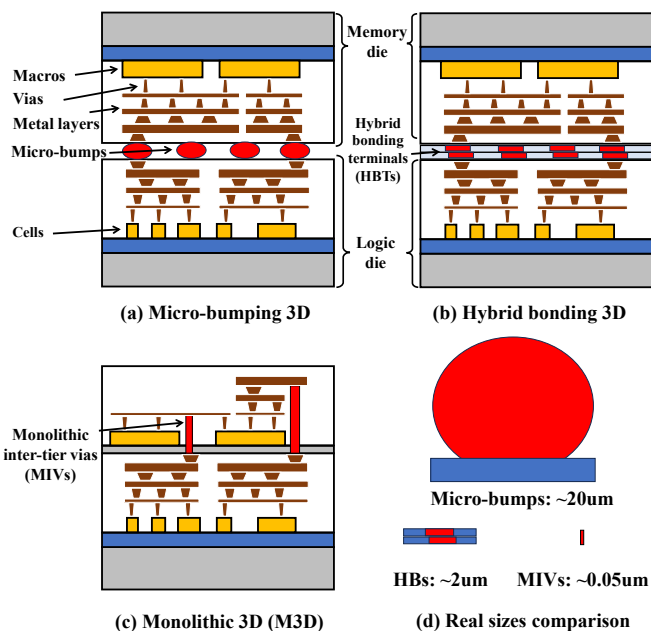


Fig. 1: The illustrations of micro-bumping, hybrid bonding, and monolithic 3D integration technologies are presented in subfigures (a), (b), and (c), respectively. The comparison of the dimensions of the three bonding vias is shown in subfigure (d).

risk of solder bridging, making them unsuitable for cutting-edge requirements [8]. Monolithic 3D (M3D) stacking, which uses MIVs (typically <100 nm) for vertical interconnections, achieves the highest inter-die connection density but is hindered by high manufacturing costs, yield issues, and quality compromises [37], [40]. In contrast, face-to-face stacking with HBTs offers a balanced solution. With a pitch around 1 μm , it meets current inter-die connection needs while enabling separate fabrication of dies, followed by annealing to form copper-to-copper bonds. This approach results in lower manufacturing complexity, higher yield, and improved reliability. Therefore, this paper focuses on face-to-face 3D stacking with HBTs.

While advanced 3D stacking technologies provide promising solutions for high-density integration, they also introduce significant challenges, particularly in managing thermal issues [31]. The severity of the challenge is influenced by the quality of placement, which decides both the distribution of cells and the subsequent routing results, two critical factors

*Equal contribution.

†Chao Qian <qianc@nju.edu.cn> is the corresponding author.

contributing to thermal generation in ICs. Furthermore, the transition from conventional 2D to 3D integration introduces an additional z-axis dimension to the placement problem, thereby exponentially increasing the complexity of the decision space and presenting significant challenges to chip design.

Over the past decade, numerous pseudo-3D and true-3D algorithms have been proposed [5], [6], [18], [38], which have achieved favorable results on various designs, metrics and evaluation flows. However, the lack of suitable benchmarks and open-source 3D implementations remains a significant issue. While the ICCAD 2022 [12] and 2023 [11] contests introduce benchmarks for 3D placement using face-to-face hybrid bonding stacking, their objectives are limited to interconnect wirelength and the number of HBTs, which are insufficient for a comprehensive evaluation of PPA (power, performance, and area) metrics. Meanwhile, several PPA-driven 3D backend flows, such as Shrunk-2D [25], Macro-3D [5], Pin-3D [26], and Art-3D [23], rely heavily on commercial 2D tools and custom in-house scripts, making them challenging to replicate and difficult to compare fairly.

To address these issues, we have developed a complete open-source 3D backend implementation benchmark based on the widely-recognized and tape-out verified OpenROAD-flow-scripts [4] (ORFS), incorporating eight designs from ORFS. This flow is highly user-friendly, supports the replacement of any component, and particularly facilitates the embedding and evaluation of any 3D placement algorithm. We hope our benchmark can help advance the field of 3D integration. Our contributions are summarized as follows:

- We propose Open3DBench¹, the first fully open-source-tool-based 3D backend implementation and PPA evaluation benchmark. It is designed to align with the advanced 3D workflow (e.g. Macro-3D [5]) that relies on commercial tools and commercial process design kits (PDKs).
- Incorporating DREAMPlace [19], we design two straightforward but effective 3D partition and placement strategies and integrate them into the complete PPA flow. One focuses on regular placement on the memory die, while the other focuses on optimizing the overall wirelength by co-optimizing the location of cells from both dies.
- Targeting the 3D face-to-face hybrid bonding stacking, we implement 3D routing, RC extraction, and 3D timing analysis, while also incorporating 3D thermal simulation to enable accurate and comprehensive PPA assessments.
- Through detailed experimental comparisons, we demonstrate that the proposed 3D framework offers significant improvements in area (51.19%), wirelength (24.06%), timing (30.84%), and power (5.72%) compared to the ORFS 2D framework. Moreover, we highlight that current 3D placement algorithms—focusing solely on wirelength optimization—are insufficient, emphasizing the necessity for further developing PPA-driven 3D methodologies.

II. RELATED WORK

Current 3D placement algorithms are generally divided into two main categories: pseudo-3D and true-3D [38]. The primary distinction lies in that—pseudo-3D methods simplify the complexity of 3D problems by reducing them to 2D and applying 2D placement techniques, while true-3D methods tackle the problem directly within the full 3D space.

Many pseudo-3D approaches focus on M3D stacking with explicit modeling and planning of MIVs. For example, Cascade-2D [6] cascades the top and bottom dies from left to right in a 2D plane and uses dummy wires and anchor cells to model inter-die connections. Fences are set as die boundaries to ensure components within their respective die. Shrunk-2D [25] halves the area of cells to enable the global placement of all components in one die. The resulting 2D layout is partitioned into uniform bins, and a min-cut algorithm is conducted within each bin to separate the top and bottom dies while maintaining area balance. After cell placement, the MIVs are inserted in the left whitespace. Compact-2D [17] improves upon Shrunk-2D by calibrating RC parasitics and introducing compact 3D via planning for post-tier partition optimization. Pin-3D [26] emphasizes the idea of pin projection that can directly integrate components in a 2D plane and further proposes 3D clock tree optimization and engineering change order (ECO) for industry-grade results.

Other pseudo-3D methods target at face-to-face hybrid bonding stacking, including Macro-3D [5] and Snap-3D [30]. Macro-3D utilizes memory-on-logic architectures and allows 2D routing tools to place HBTs in a way similar to vias. This is achieved by stacking the metal layers of both the top and bottom dies within a single integrated design. Snap-3D extends the support for cell placement on both dies by halving cell heights and utilizing 2D tools to place cells in one die. The cells partitioned to the top tier are placed onto the rows marked top, and the bottom tier cells go to the bottom rows. The strengths of these works lie in their use of real-world designs, industrial-grade tools, and a comprehensive PPA evaluation flow. However, a major drawback remains: the closed-source nature of the tools and scripts makes fair replication and comparison difficult, limiting further exploration by the academic community and creating a high barrier for newcomers.

True-3D works basically employ analytical methods, performing placement in a 3D cuboid region based on smoothed wirelength and density models. Representative works include NTUPlace3-3D [10], which utilizes a bell-shaped density model considering TSV insertion, and ePlace-3D [21], which models the density constraint as a 3D electrostatic field. More recently, Analytical-3D [18] uses a bistratal wirelength model to enhance the accurate approximation of 3D wirelength, and Zhao et al. [38] implement a preconditioning operator on this basis to support mixed-size 3D placement of macros and standard cells. Art-3D [23] integrates an academic true-3D placement engine with a commercial tool-based PPA evaluation, which still suffers from the closed nature. Another recent work, TA-3D [15], proposes a framework that enables

¹<https://github.com/lamda-bbo/Open3DBench>

TABLE I: Qualitative comparison between representative 3D flows and Open3DBench.

Method	Shrunk-2D [25]	Macro-3D [5]	Art-3D [23]	Analytical-3D [18]	TA-3D [15]	Open3DBench
Partition	Min-cut	Mem-on-logic	Do while place	Do while place	Graph embedding-based clustering	Mem-on-logic and compatible with others
Macro Placement	2D commercial	Hand-crafted	Do with cells	Not supported	Not supported	Two dies co-optimization
Cell Placement	2D commercial	2D commercial	True-3D	True-3D	True-3D	Two dies co-optimization
Place Optimization	Not supported	Not supported	2D commercial	Not supported	Not supported	OpenROAD
Routing	Die-by-die	3D metal stack	3D metal stack	Not supported	Not supported	3D metal stack
Evaluation	PPA	PPA	PPA	HPWL + HBT cost	Post-place PPA	PPA + Thermal
Open PDK	No	No	No	Not supported	Yes	Yes
Open Designs	Yes	Yes	Partially	Yes	Yes	Yes
Open Source Code	No	No	No	No	No	Yes

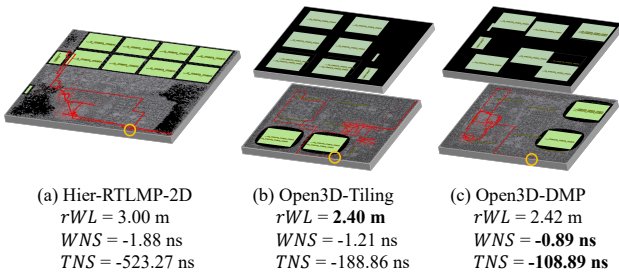


Fig. 2: Comparison of routing wirelength (rWL), WNS, and TNS on design `bp_be`. Results generated by 2D and 3D flows using Hier-RTLMP-2D, Open3D-Tiling and Open3D-DMP methods for macro placement are presented in subfigures (a), (b), and (c), respectively. The red path highlights the most critical datapath, where the corresponding slack equals the WNS. All three paths originate from the same flip-flop and terminate at the same output port, indicated by a yellow circle.

timing-aware partitioning and true-3D placement. However, its timing analysis is restricted to the placement stage, relying on Steiner trees for estimating routing results. This approach, while practical, lacks sufficient accuracy for designs with limited routing resources.

Most true-3D placement methodologies rely on academic benchmarks (e.g., ICCAD 2022 [12], 2023 [11]) and primarily focus on wirelength as the key optimization objective without performing a comprehensive PPA evaluation. This results in a notable gap between wirelength optimization and final PPA outcomes, a limitation that has also been highlighted in 2D scenarios [29], [32], [35]. To demonstrate this issue, we present a case study in Fig. 2. Compared to the conventional 2D design flow, 3D methods consistently achieve improvements in both wirelength and timing. However, when comparing Open3D-Tiling and Open3D-DMP—two implementations of 3D placement in our framework—better wirelength does not always lead to improved worst slack or total slack.

The lack of openness and the complexity of implementing PPA evaluation flows remain significant challenges in developing advanced 3D EDA methodologies. To tackle this, we present Open3DBench, a fully open-source, user-friendly

3D evaluation framework. It includes default implementations for 3D partitioning and placement, which can be seamlessly replaced with any customized algorithm, enabling standardized and reproducible evaluations. A qualitative comparison between representative 3D design flows and Open3DBench is provided in Table I.

III. FLOW IMPLEMENTATION

Open3DBench is developed entirely using open-source tools, PDKs, and designs, as illustrated in Fig. 3. We have made targeted adjustments and modifications to align with advanced 3D backend design frameworks, typically those reliant on commercial tools, PDKs, and in-house scripts [5], [16]. Our flow enables comprehensive and accurate PPA evaluation, including 3D timing and power analysis.

Notably, our flow incorporates dedicated support for 3D placement algorithms. It facilitates the seamless extraction of 3D netlists, which can be directly utilized by any 3D placement algorithm to produce 3D placement *def* results. These results can then be integrated into the complete PPA evaluation flow for comprehensive comparison or further PPA-driven optimization.

A. PDK Preparation

To describe the technologies and physical properties of 3D designs, we modify the original 2D PDK Nangate45 [28] to create a 3D version, referred to as Nangate45_3D. The key modifications involve adjustments to the *techlef* and *lef* files.

The *techlef* defines the physical properties of all metal and via layers, serving as the foundational basis for face-to-face bonding in 3D integration. The original Nangate45 *techlef* includes 10 metal layers, ranging from the lowest metal_1 to the highest metal_10, with increasing wire width and pitch. To enable the representation of 3D routing resources using existing 2D tools, we duplicate metal_1 through metal_10, including all via layers, and invert them above metal_10, resulting in a symmetric structure: metal_10 paired with metal_11, metal_9 with metal_12, and so forth, up to metal_1 paired with metal_20. In this configuration, metal_1–10 are associated with the bottom die, while metal_20–11 correspond

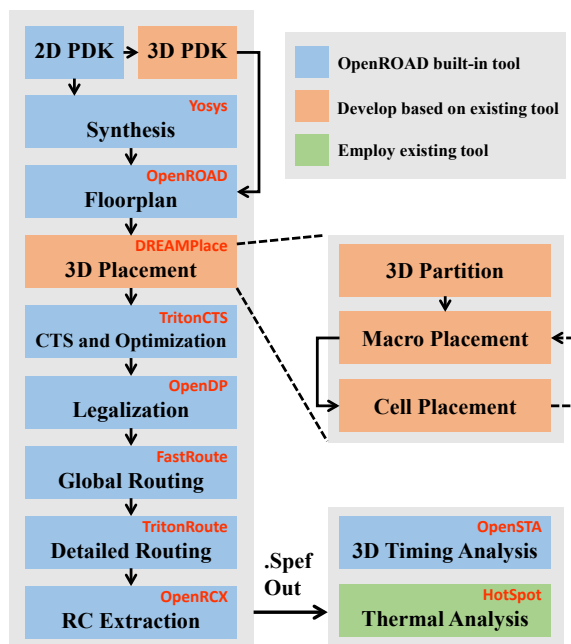


Fig. 3: Overview of the proposed 3D backend implementation flow. The specific open-source tool adopted for each stage is marked in red.

to the top die. Additionally, we introduce an HBT layer for inter-die connection, with each HBT defined as a $0.5 \mu\text{m} \times 0.5 \mu\text{m}$ square with a pitch of $1.5 \mu\text{m}$, connecting metal₁₀ and metal₁₁ to establish a physical link between two dies.

The LEF files provide geometric and pin information for each macro and cell. To distinguish components located on the top and bottom dies, each library component is divided into two types of cells, with the suffix “_top” or “_bottom” added to their names. For example, the standard cell “Buffer_X16” is divided into “Buffer_X16_top” and “Buffer_X16_bottom”. For components implemented on the top die, their pins and routing obstructions are both adjusted accordingly to the top die layers, while components on the bottom die retain their original layer definitions. To enable 2D tools to process both dies simultaneously (e.g., during gate sizing or buffer insertion), the layout of the top die must either be hidden or treated as transparent to prevent spatial conflicts. To achieve this, a “shrunk” *lef* class is introduced to define the “transparent” components, where the height of each cell or macro is reduced to a single-row height ($1.4 \mu\text{m}$), the width is shrunk to the site width ($0.19 \mu\text{m}$), while all pins are preserved for compatibility with routing processes.

B. Synthesis and Floorplan

We leverage the built-in synthesis scripts provided by ORFS and utilize the 2D Nangate45 [28] PDK, employing Yosys [34] to generate the 2D netlist. Note that the 3D netlist is constructed in the subsequent 3D tier partition stage. During the floorplan phase, random input-output (I/O) port placement is performed. Due to the reduced die size, I/O placement constraints are relaxed to mitigate potential I/O

resource shortages. All I/O ports are initially assigned to the bottom die and will be adjusted based on the tier partitioning results. Specifically, the tier of each I/O port is determined by the tier of its connected pin.

C. 3D Tier Partition

In the design of 3D-ICs, the original 2D netlist must be partitioned into two or more subparts that are assigned to different dies. Our proposed flow focuses primarily on the memory-on-logic partition, which locates memory blocks on the top die and assigns logic cells on the bottom die. Modern chip designs like microprocessors and accelerators usually incorporate large memory blocks that occupy a significant proportion of the layout area, thereby obstructing or prolonging the signal paths between logic cells [27]. The use of memory-on-logic partitioning can directly address this issue.

When macros occupy much more space than cells, some top-die memory blocks should be relocated to the logic die for more balanced area utilization. In this relocation process, we minimize the number of nets that span two dies, i.e., minimize the cut edges, to reduce the cost of using HBTs and avoid the potential overlaps between the HBTs [18]. Therefore, the optimization function of memory relocation (i.e., memory partitioning) involves the weighted average of the cut value and the difference in area utilization between the top and bottom dies. We employ a simple evolutionary algorithm [39] with binary solution representation, where each bit corresponds to the assignment of a certain macro: “1” represents the top die and “0” represents the bottom die. It utilizes bitwise mutation to generate neighboring solutions in each iteration, and the generated solutions with worse fitness can survive with a gradually decreasing probability. After the optimization process, the components are properly separated to form a 3D design while maintaining the area balance.

Beyond the memory-on-logic partition, the proposed flow also supports the PPA evaluation of mixed partition results, i.e., both dies have memory blocks and logic cells. However, the experimental evaluation of mixed partition is not included by the limitations of current 2D analytical placement tools, primarily due to the challenge in tackling the overlap of macros and the projected cells from the other die. It is noteworthy that the subsequent stages of our proposed flow, including clock tree synthesis (CTS), routing, and RC extraction, demonstrate full compatibility with logic cells from both dies.

D. Placement

Following the 3D tier partition, a 3D placement process is required to optimize the coordinates for both macros and standard cells. To address macro placement systematically, we implement and evaluate two strategies: (1) Tiling strategy. This strategy aims to regularly place the macros in an array-like layout. (2) An analytical method that utilizes mixed-size placement and extracts macro positions from the results.

1) *Macro placement by tiling*: Our tiling implementation employs the skyline packing algorithm [33] with size-ordered macro sequencing, which places each subsequent macro at the

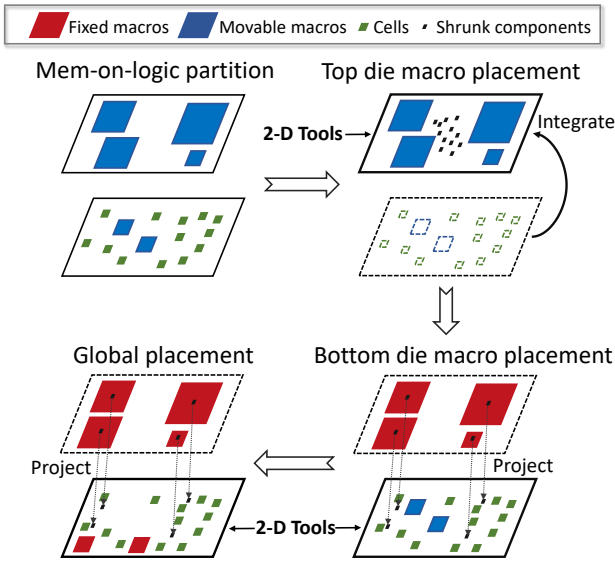


Fig. 4: Illustration of our analytical pseudo-3D placement process. In each stage, the 2D placement is performed on the 2D plane framed by the solid line, where the components of the other die are integrated or projected onto the target die.

leftmost position of the lowest available skyline. To adequately utilize the memory die, the halo around the macro is adaptively increased to make the highest macro exceed 80% of the die height. After macro positions are fixed, we project the top-die macros to the bottom die with a shrunk size and perform cell placement on the 2D bottom die by DREAMPlace [19].

2) *Analytical pseudo-3D placement:* While the tiling strategy provides a structured baseline, we further develop an analytical pseudo-3D placement framework that considers connectivity across both memory and logic dies. This placement flow involves macro placement for two dies and global placement for logic cells, as illustrated in Fig. 4. To accommodate the strong correlation between the positions of macros and standard cell clusters [36], we incorporate the macro-cell connectivity into the macro placement process to enhance the performance of the final global placement. The complete pipeline includes three steps: top die macro placement, bottom die macro placement, and global placement, as detailed below:

a) *Top Die Macro Placement:* We scale the sizes of the standard cells and macros on the bottom die to a minimal number and integrate all the bottom-die components to the top die. Subsequently, DREAMPlace is invoked to optimize the coordinates of all components in the 2D plane. Only the positions of the top-die macros are retained as a result.

b) *Bottom Die Macro Placement:* We scale down the top-die macros' size to a minimal number while keeping their pin positions unchanged and project them to the bottom die. Then, the 2D placement tool is called to place all other components on the bottom die. In this stage, we extract the positions of the bottom-die macros as a result.

c) *Global Placement:* After the positions of the macros on both dies are fixed, we project top-die macros to the bottom

die as described in the step b). Subsequently, DREAMPlace is used to complete the placement of bottom-tie standard cells.

E. Placement Optimization and CTS

After the initial placement, backend optimizations are conducted to address timing and design rule violations (DRVs), using buffer insertion and gate resizing. All the buffers are first inserted to the die with more standard cells. Each buffer is then assigned to the die containing the majority of its driving components. For cells on the top die, the previously described shrunk *lef* class is used to make them physically transparent to the bottom die while retaining all pin information. This approach prevents spatial interference with resizing and buffer insertion on the bottom die. During the resizing process, the placement tool uses cell information from both dies, which can result in scenarios where a cell, such as “INV_X4_bottom” is resized to “INV_X16_top”. To handle this, the die assignment of each cell is recorded during the partitioning stage, and the suffix is updated accordingly after placement optimization.

For CTS, we adopt the default settings of ORFS and construct the clock tree on the die with more standard cells (bottom die in our experiments), considering the lower cross-die cost. Once all optimizations are complete and the correct die assignment for each cell is ensured, the *def* files for the top and bottom dies are loaded separately. At this stage, all cells are restored to their actual sizes. Legalization is then performed for each die to ensure that the layouts are valid.

F. 3D Routing with 2D Tool

Since the *techlef* encompasses all metal layers for both dies as well as the HBT layer connecting them, 2D routing tools can accurately capture the complete 3D routing information. Global and detailed routing are performed using FastRoute [24] and TritonRoute [14], respectively. Although the physical properties of HBTs—such as their size ($0.5 \mu\text{m} \times 0.5 \mu\text{m}$) and pitch ($1 \mu\text{m}$)—are properly defined, we observe that HBT overlaps can still occur during routing. This issue arises because current routers treat HBTs like vias, despite their significantly larger footprint compared to standard vias and track pitches, as noted by Liu et al. [20]. In future work, we will integrate HBT-aware routing methods [20] into our flow to address this issue.

G. RC Extraction and Static Timing Analysis (STA)

OpenROAD's built-in OpenRCX [2] is utilized for RC extraction, which requires golden rules to characterize the parasitics of each metal layer. However, with the doubling of metal layers in 3D designs, the default rules for Nangate45 are no longer applicable. To address this, we first generate the golden *spef* for the modified *techlef* using commercial tools. Subsequently, OpenRCX is employed to extract 3D golden rules from the *spef*. These rules are then integrated into the 3D PDK, facilitating RC extraction and enabling the generation of the final *spef* after the routing stage. The resulting *spef* is fed into OpenSTA [3] to evaluate the 3D timing performance.

TABLE II: Post-route PPA results on eight designs, where best results are in **bold**.

Designs	Methods	Area (mm ²)	rWL (m)	Overflow (#)	WNS (ns)	TNS (ns)	Power (W)	T _{max} (°C)	Runtime (s)
ariane133	Hier-RTLMP-2D	2.25	8.20	132	-2.18	-5766.41	0.393	58.84	3667
	DREAMPlace-2D	2.25	7.18	112	-1.69	-4098.04	0.389	58.69	1556
	Open3D-Tiling	1.00	6.21	0	-1.40	-3049.41	0.360	58.35	1743
	Open3D-DMP	1.00	5.59	0	-1.34	-2648.76	0.360	58.21	1739
ariane136	Hier-RTLMP-2D	2.25	8.63	127	-2.51	-7072.67	0.514	63.40	1779
	DREAMPlace-2D	2.25	7.80	148	-2.71	-7561.23	0.508	61.14	1720
	Open3D-Tiling	1.00	6.32	0	-2.38	-6125.24	0.471	60.93	1791
	Open3D-DMP	1.00	6.05	0	-2.45	-6603.91	0.471	62.27	1870
black_parrot	Hier-RTLMP-2D	1.76	12.41	68	-6.96	-6289.17	0.398	55.14	1819
	DREAMPlace-2D	1.76	12.23	334	-6.57	-5268.85	0.399	55.26	1728
	Open3D-Tiling	0.81	8.08	0	-5.76	-2251.30	0.376	62.29	1895
	Open3D-DMP	0.81	7.79	0	-5.67	-4067.11	0.374	60.97	1920
bp_be	Hier-RTLMP-2D	0.56	3.00	30	-1.88	-523.27	0.152	52.63	1063
	DREAMPlace-2D	0.56	2.89	36	-1.30	-246.99	0.153	53.08	916
	Open3D-Tiling	0.30	2.40	0	-1.21	-188.86	0.144	61.17	998
	Open3D-DMP	0.30	2.42	0	-0.89	-108.89	0.144	59.11	1053
bp_fe	Hier-RTLMP-2D	0.48	1.81	6	-1.40	-942.36	0.302	64.09	449
	DREAMPlace-2D	0.48	1.73	30	-1.51	-978.59	0.305	63.62	239
	Open3D-Tiling	0.24	1.38	0	-1.53	-729.42	0.284	87.33	398
	Open3D-DMP	0.24	1.30	0	-1.37	-814.64	0.283	82.32	388
bp_multi	Hier-RTLMP-2D	1.21	6.20	36	-7.97	-12072.10	1.143	86.18	868
	DREAMPlace-2D	1.21	5.63	9	-8.30	-10946.20	1.126	85.50do	760
	Open3D-Tiling	0.64	4.06	0	-7.01	-9246.70	1.062	112.09	883
	Open3D-DMP	0.64	4.03	0	-8.03	-9812.57	1.050	98.09	935
bp_quad	Hier-RTLMP-2D	12.96	46.63	3429	-3.66	-39020.00	1.822	66.05	8010
	DREAMPlace-2D	12.96	41.99	3968	-2.05	-31231.90	1.848	68.17	6336
	Open3D-Tiling	6.25	50.19	0	-2.62	-31124.70	1.840	69.78	7973
	Open3D-DMP	6.25	40.39	0	-1.83	-26966.20	1.832	66.96	7981
swerv_wrapper	Hier-RTLMP-2D	1.10	5.62	14428	-2.14	-1975.79	0.250	54.86	1175
	DREAMPlace-2D	1.10	5.54	9540	-1.86	-1429.90	0.254	53.48	1092
	Open3D-Tiling	0.56	3.63	0	-1.26	-972.80	0.232	62.17	2085
	Open3D-DMP	0.56	3.46	0	-1.23	-958.01	0.234	60.49	1744
3D improvements over 2D†		51.19%↑	24.06%↑	100%↑	16.24%↑	30.84%↑	5.72%↑	-10.04%↓	-24.82%↓
3D-DMP improvements over 3D-Tiling		Equal	5.96%↑	Equal	7.22%↑	-4.49%↓	1.98%↑	3.56%↑	0.23%↑

†We compare the best results from two 2D methods with those from two 3D methods, and report the average improvement across 8 designs.

TABLE III: Detailed statistics of eight designs. Freq. represents the clock frequency of the design.

Designs	# Macro	# Net	# Cell	Freq. (MHz)
ariane133	132	204K	168K	250.0
ariane136	136	209K	171K	333.3
black_parrot	24	359K	307K	500.0
bp_be	10	66K	51K	1250.0
bp_fe	11	43K	33K	555.6
bp_multi	26	179K	152K	1250.0
bp_quad	220	1448K	1135K	384.6
swerv_wrapper	28	117K	98K	500.0

H. Thermal Simulation

We use HotSpot 7.0 [1], [9] for thermal simulation. To balance efficiency and accuracy, the layout is divided into a 10 × 10 grid, with power consumption aggregated for each grid per die. In our experiments, the same method is applied to 2D designs, enabling a fair comparison to assess if transitioning from 2D to 3D designs introduces significant thermal issues.

IV. EXPERIMENTS

We implement our 3D framework based on the latest OpenROAD commit². We use eight RTL designs from the OpenROAD-flow-scripts³ repository, synthesized with the Nangate45 library [28]. Detailed statistics of our designs are listed in Table III. To enable a timing performance comparison, we increase the frequency of designs without violating timing paths. Our 3D placement engine is modified from the released version⁴ of DREAMPlace 4.1.0 [7]. All the evaluations are run on a Linux server with a 52-core Intel Xeon CPU@2.60 GHz, an NVIDIA RTX 2080S GPU, and 128GB RAM.

A. ORFS 2D Flow vs. Open3DBench

The main results are presented in Table II. For comparative analysis, we implement two baseline methodologies integrated with a comprehensive ORFS 2D RTL-to-GDS flow. The process begins with ORFS default synthesis flow to generate 2D netlists, followed by floorplanning to establish

²<https://github.com/The-OpenROAD-Project/OpenROAD/commit/fbca14c>

³<https://github.com/The-OpenROAD-Project/OpenROAD-flow-scripts>

⁴<https://github.com/limbo018/DREAMPlace/releases/tag/4.1.0>

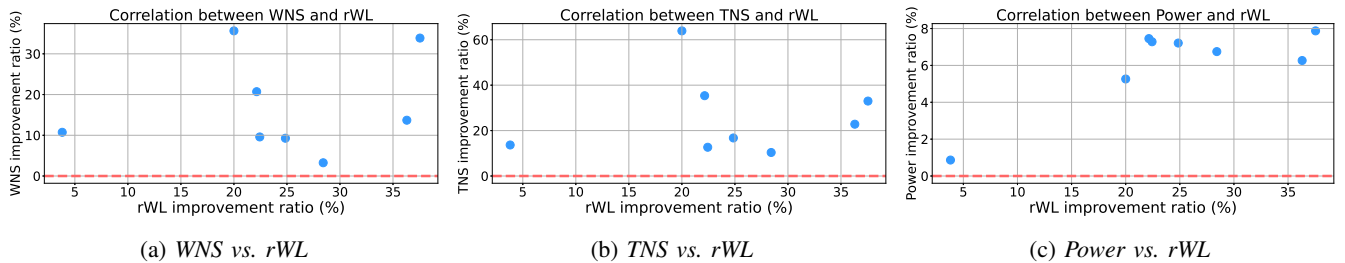


Fig. 5: Correlation analysis between rWL and key performance metrics comparing 2D and 3D methods. We plot the improvement ratio of the 3D method with the best rWL compared to the 2D method with the best rWL.

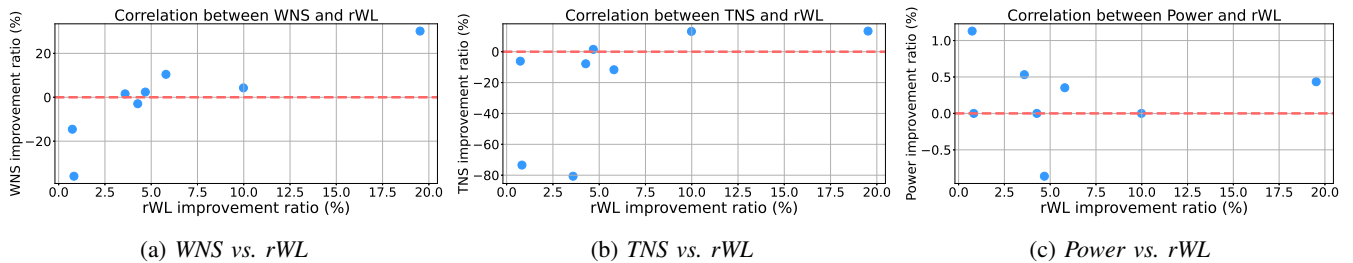


Fig. 6: Correlation analysis between rWL and key performance metrics comparing two 3D methods. We plot the improvement ratio of the 3D method with better rWL compared to the other 3D method.

initial pin assignments. Subsequently, we employ either Hier-RTLMP [13] or DREAMPlace 4.1.0 [7] for macro placement, denoted as Hier-RTLMP-2D and DREAMPlace-2D in Table II, respectively. Then we fix the macros, and place standard cells using DREAMPlace 4.1.0. The evaluation flow encompasses sequential stages of placement optimization, CTS, routing, RC extraction, final STA, and HotSpot thermal simulation to provide comprehensive PPA assessment. Our proposed 3D placement methodologies detailed in Sec. III-D, are denoted as Open3D-Tiling and Open3D-DMP.

For each 3D design, we reduce the original die area by about 50% through the two-tier stacking. To evaluate performance, we compare the best results from two 2D methods with those from two 3D methods across eight designs, calculating the average improvement ratios for each metric, as presented in the penultimate row of Table II. The results clearly demonstrate that 3D methods consistently outperform 2D approaches across key metrics, including routing wirelength (rWL), global routing overflow (Overflow), worst negative slack (WNS), total negative slack (TNS), and power consumption, for all eight designs. The only exception is `bp_quad`, where Hier-RTLMP-2D achieves better power efficiency.

A significant improvement is observed in rWL, a critical objective due to its correlation with key performance metrics. The 3D flow achieves an average 24.06% enhancement in rWL compared to 2D methods. This improvement primarily stems from the support of vertical connections and mem-on-logic architecture, which effectively eliminates macro blockages that typically cause substantial routing detours. This architectural advantage also contributes to completely overflow-free routing results in the 3D flow. The comprehensive 3D metal stack enables the STA engine to precisely model the parasitics

of HBTs, metal wires, and vias, together with significant wirelength improvement, leading to notable advancements in timing metrics compared to 2D methods. We also achieve a 5.72% improvement in power efficiency, which may seem modest but is highly significant in today’s industry where low-power design is increasingly critical. The optimized wirelength contributes to this improvement by not only reducing power dissipation in interconnect metals but also minimizing the need for buffer insertion and large driving cells, which are typically associated with higher power consumption.

B. 3D Macro Tiling vs. 3D Mixed-size Placement

Sec. III-D introduces two 3D placement approaches. Open3D-Tiling prioritizes regular macro placement without considering interconnect optimization, while Open3D-DMP enhances wirelength performance by co-optimizing cells across both dies. Experimental results demonstrate Open3D-DMP’s advantages: It achieves superior wirelength in seven out of eight test cases with an average 5.96% improvement compared to Open3D-Tiling. However, the wirelength optimization does not bring consistent improvement over PPA metrics, WNS, TNS, and power. We can observe that WNS and power are improved by 7.22% and 1.98%, respectively, while TNS gets worse by a ratio of 4.49%. These observations motivate our subsequent correlation analysis in Sec. IV-C.

C. Correlation Study between rWL and PPA Metrics

Routing wirelength has long been a primary objective in chip placement optimization. Fig. 5 demonstrates that when comparing the best-rWL 3D method with the best-rWL 2D method across all eight designs, significant improvements

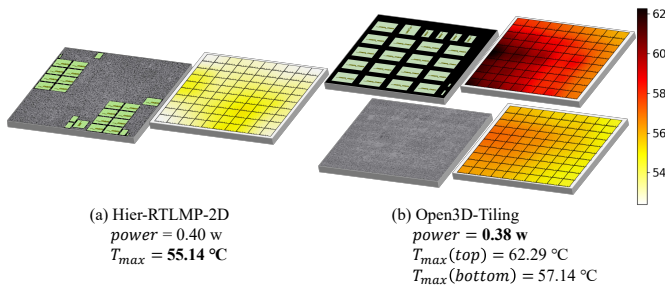


Fig. 7: Heat map visualization of Hier-RTLMP-2D and Open3D-Tiling on design `black_parrot`. While the 3D-IC architecture achieves reduced power consumption, it exhibits a higher peak temperature due to increased integration density.

in rWL (around 25%) often correlate positively with enhancements in key performance metrics: WNS, TNS, and power consumption, as shown in subfigures 5a, 5b, and 5c, respectively. The red dotted line in each subfigure represents the zero borderline. Any scatter below this line suggests that improvements in wirelength do not benefit the PPA metrics. We can conclude from Fig. 5 that substantial improvements in rWL are likely to positively impact timing performance and power, although the extent varies by design.

The scenario, however, changes when the improvement in rWL is moderate, as illustrated in Fig. 6. Here, we use the 3D method with worse rWL result as a baseline for each design and compare it against the other method. Several scatters in the three subfigures lie below the red line, indicating that even when rWL shows superiority, improvements in WNS, TNS, or power are not guaranteed. This is likely because the wirelength differences between 3D methods are not significant, with only one case `bp_quad` showing a 20% improvement, while the remaining seven designs show improvements of 10% or less, which is insufficient to ensure PPA superiority.

In summary, optimizing wirelength remains a necessary goal in chip placement. However, when optimization techniques only achieve marginal improvements (e.g. less than five percent), the anticipated PPA benefits may not be realized. This underscores the importance of developing PPA-oriented methodologies that simultaneously address final performance metrics and maintain wirelength optimization considerations, which fundamentally highlights the value of our proposed open-source 3D evaluation benchmark.

D. Thermal Issue

Thermal management has emerged as a critical challenge in 3D-IC design [31]. Open3DBench thus integrates an efficient 3D thermal simulation framework, aiming to further support thermal-aware EDA methods. To generate more pronounced temperature variations, we scale the power consumption of each component by a factor of ten during the simulation. This adjustment is necessary because the original power values result in temperature differences that are too subtle to effectively distinguish the intensity of thermal effects. As quantitatively demonstrated in Table II and visually represented in Fig. 7,

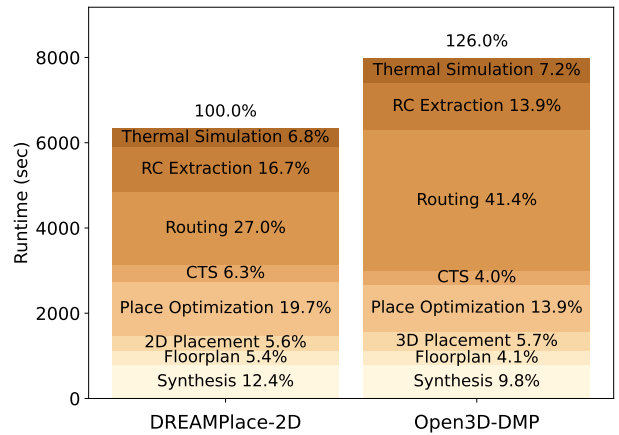


Fig. 8: Runtime breakdown comparison between DREAMPlace-2D and Open3D-DMP for case `bp_quad`. The time spent by each component is normalized by 6336 seconds, the total runtime of DREAMPlace-2D.

our results clearly reveal the thermal issues of 3D-IC designs. Specifically, 3D designs demonstrate a 10.04% higher peak temperature compared to their 2D counterparts, which can be directly attributed to the increased component density within a more compact footprint.

E. Runtime Breakdown

We report the runtime of four methods across eight designs in Table II, showing that 3D methods have an additional runtime overhead of 24.82% compared to the 2D method DREAMPlace-2D. To analyze this, we break down the runtime in Fig. 8, comparing DREAMPlace-2D and Open3D-DMP on the largest design, `bp_quad` (over one million gates). The main overhead in 3D methods comes from detailed routing, as doubling the metal layers to 20 requires more time for design rule checks (DRCs) and optimizations. Note that Hier-RTLMP-2D even consumes more time than 3D methods, primarily due to the high cost of its macro placement method.

V. CONCLUSION AND FUTURE WORK

This paper presents Open3DBench, an open-source benchmark for 3D-IC backend implementation and PPA evaluation, built upon the widely adopted OpenROAD-flow-scripts. By integrating modular 3D partitioning and placement, 3D routing, RC extraction, and thermal simulation, the framework enables comprehensive PPA evaluation of 3D design methodologies. Experimental results validate significant wirelength, area, timing and power improvements over 2D flows, yet highlight that wirelength-centric optimization alone inadequately ensures PPA gains. Open3DBench addresses the critical need for accessible 3D benchmarking by bridging the gaps posed by custom in-house scripts and costly commercial tools, offering standardized workflows and PDK compatibility.

Current limitations include HBT overlaps, thermal issues, and restricted support for heterogeneous designs. Future efforts can prioritize extension to HBT assignment, PPA-driven optimization, and broader adoption of advanced 3D techniques.

REFERENCES

- [1] “HotSpot,” <https://github.com/uvahotspot/HotSpot>.
- [2] “OpenRCX,” <https://github.com/The-OpenROAD-Project/OpenRCX>.
- [3] “OpenSTA,” <https://github.com/parallaxsw/OpenSTA>.
- [4] T. Ajayi, D. Blaauw, T. Chan, C. Cheng, V. Chhabria, D. Choo, M. Coltellà, S. Dobre, R. Dreslinski, M. Fogaça *et al.*, “OpenROAD: Toward a self-driving, open-source digital layout implementation tool chain,” in *Proceedings of Government Microcircuit Applications and Critical Technology Conference*, Albuquerque, NM, 2019, pp. 1105–1110.
- [5] L. Bamberg, A. García-Ortiz, L. Zhu, S. Pentapati, S. K. Lim *et al.*, “Macro-3D: A physical design methodology for face-to-face-stacked heterogeneous 3D ICs,” in *Proceedings of Design, Automation & Test in Europe Conference*, Grenoble, France, 2020, pp. 37–42.
- [6] K. Chang, S. Sinha, B. Cline, R. Southerland, M. Doherty, G. Yeric, and S. K. Lim, “Cascade2D: A design-aware partitioning approach to monolithic 3D IC with 2D commercial tools,” in *Proceedings of IEEE/ACM International Conference on Computer-Aided Design*, Austin, TX, 2016, pp. 1–8.
- [7] Y. Chen, Z. Wen, Y. Liang, and Y. Lin, “Stronger mixed-size placement backbone considering second-order information,” in *Proceedings of IEEE/ACM International Conference on Computer-Aided Design*, San Francisco, CA, 2023, pp. 1–9.
- [8] J. Derakhshandeh, L. Hou, I. De Preter, C. Gerets, S. Suhand, V. Dubey, G. Jamieson, F. Inoue, T. Webers, P. Bex, G. Capuz, E. Beyne, J. Slabbeboom, T. Wang, A. Jourdain, G. Beyer, K. June Rebibis, and A. Miller, “Die to wafer 3D stacking for below 10um pitch microbumps,” in *Proceedings of IEEE International 3D Systems Integration Conference*, San Francisco, CA, 2016, pp. 1–4.
- [9] J.-H. Han, X. Guo, K. Skadron, and M. R. Stan, “From 2.5D to 3D chiplet systems: Investigation of thermal implications with HotSpot 7.0,” in *Proceedings of IEEE Intersociety Conference on Thermal and Thermomechanical Phenomena in Electronic Systems*, San Diego, CA, 2022, pp. 1–6.
- [10] M.-K. Hsu, V. Balabanov, and Y.-W. Chang, “TSV-aware analytical placement for 3-D IC designs based on a novel weighted-average wirelength model,” *IEEE Transactions on Computer-Aided Design of Integrated Circuits and Systems*, vol. 32, no. 4, pp. 497–509, 2013.
- [11] K.-S. Hu, H.-Y. Chi, I.-J. Lin, Y.-H. Wu, W.-H. Chen, and Y.-T. Hsieh, “2023 ICCAD CAD contest problem B: 3D placement with macros,” in *Proceedings of IEEE/ACM International Conference on Computer-Aided Design*, San Francisco, CA, 2023, pp. 1–6.
- [12] K.-S. Hu, I.-J. Lin, Y.-H. Huang, H.-Y. Chi, Y.-H. Wu, and C.-F. C. Shen, “2022 ICCAD CAD contest problem B: 3D placement with D2D vertical connections,” in *Proceedings of IEEE/ACM International Conference on Computer-Aided Design*, New York, NY, 2022, pp. 1–5.
- [13] A. B. Kahng, R. Varadarajan, and Z. Wang, “Hier-RTLMP: A hierarchical automatic macro placer for large-scale complex IP blocks,” *IEEE Transactions on Computer-Aided Design of Integrated Circuits and Systems*, vol. 43, no. 5, pp. 1552–1565, 2024.
- [14] A. B. Kahng, L. Wang, and B. Xu, “TritonRoute: The open-source detailed router,” *IEEE Transactions on Computer-Aided Design of Integrated Circuits and Systems*, vol. 40, no. 3, pp. 547–559, 2021.
- [15] D. Kim, M. Kim, J. Hur, J. Lee, J. Cho, and S. Kang, “TA3D: Timing-aware 3D IC partitioning and placement by optimizing the critical path,” in *Proceedings of the ACM/IEEE International Symposium on Machine Learning for CAD*, New York, NY, 2024, pp. 1–7.
- [16] J. Kim, L. Zhu, H. M. Torun, M. Swaminathan, and S. K. Lim, “Micro-bumping, hybrid bonding, or monolithic? A PPA study for heterogeneous 3D IC options,” in *Proceedings of ACM/IEEE Design Automation Conference*, San Francisco, CA, 2021, pp. 1189–1194.
- [17] B. W. Ku, K. Chang, and S. K. Lim, “Compact-2D: A physical design methodology to build commercial-quality face-to-face-bonded 3D ICs,” in *Proceedings of the International Symposium on Physical Design*, Monterey, CA, 2018, pp. 90–97.
- [18] P. Liao, Y. Zhao, D. Guo, Y. Lin, and B. Yu, “Analytical die-to-die 3-D placement with bistratal wirelength model and GPU acceleration,” *IEEE Transactions on Computer-Aided Design of Integrated Circuits and Systems*, vol. 43, no. 6, pp. 1624–1637, 2024.
- [19] Y. Lin, S. Dhar, W. Li, H. Ren, B. Khailany, and D. Z. Pan, “DREAM-Place: Deep learning toolkit-enabled GPU acceleration for modern VLSI placement,” in *Proceedings of ACM/IEEE Design Automation Conference*, Las Vegas, NV, 2019, pp. 1–6.
- [20] S. Liu, J. Jiang, Z. He, Z. Wang, Y. Lin, B. Yu, and M. Wong, “Routing-aware legal hybrid bonding terminal assignment for 3D face-to-face stacked ICs,” in *Proceedings of the International Symposium on Physical Design*, Taipei, Taiwan, 2024, pp. 75–82.
- [21] J. Lu, H. Zhuang, I. Kang, P. Chen, and C.-K. Cheng, “ePlace-3D: Electrostatics based placement for 3D-ICs,” in *Proceedings of the International Symposium on Physical Design*, Santa Rosa, CA, 2016, pp. 11–18.
- [22] G. Moore, “Cramming more components onto integrated circuits,” *Proceedings of the IEEE*, vol. 86, no. 1, pp. 82–85, 1998.
- [23] G. Murali, S. M. Shaji, A. Agnesina, G. Luo, and S. K. Lim, “Art-3D: Analytical 3D placement with reinforced parameter tuning for monolithic 3D ICs,” in *Proceedings of the International Symposium on Physical Design*, Virtual, Canada, 2022, pp. 97–104.
- [24] M. Pan and C. Chu, “FastRoute: A step to integrate global routing into placement,” in *Proceedings of IEEE/ACM International Conference on Computer Aided Design*, San Jose, CA, 2006, pp. 464–471.
- [25] S. Panth, K. Samadi, Y. Du, and S. K. Lim, “Shrunk-2-D: A physical design methodology to build commercial-quality monolithic 3-D ICs,” *IEEE Transactions on Computer-Aided Design of Integrated Circuits and Systems*, vol. 36, no. 10, pp. 1716–1724, 2017.
- [26] S. S. K. Pentapati, K. Chang, V. Gerousis, R. Sengupta, and S. K. Lim, “Pin-3D: A physical synthesis and post-layout optimization flow for heterogeneous monolithic 3D ICs,” in *Proceedings of IEEE/ACM International Conference on Computer-Aided Design*, San Diego, CA, 2020, pp. 1–9.
- [27] Y. Pu, T. Chen, Z. He, C. Bai, H. Zheng, Y. Lin, and B. Yu, “In-crcMacro: Incremental macro placement refinement,” in *Proceedings of the International Symposium on Physical Design*, Taipei, Taiwan, 2024, pp. 169–176.
- [28] A. Rob, “Nangate technology node,” <https://si2.org/open-cell-library/>.
- [29] Y. Shi, S. Xu, S. Kai, X. Lin, K. Xue, M. Yuan, and C. Qian, “Timing-driven global placement by efficient critical path extraction,” in *Proceedings of Design, Automation & Test in Europe Conference*, Lyon, France, 2025, in press.
- [30] P. Vanna-Iampikul, C. Shao, Y.-C. Lu, S. Pentapati, and S. K. Lim, “Snap-3D: A constrained placement-driven physical design methodology for face-to-face-bonded 3D ICs,” in *Proceedings of the International Symposium on Physical Design*, Virtual, USA, 2021, pp. 39–46.
- [31] Q. Wang, X. Li, T. Jia, Y. Lin, R. Wang, and R. Huang, “ATPlace2.5D: Analytical thermal-aware chiplet placement framework for large-scale 2.5D-IC,” in *Proceedings of IEEE/ACM International Conference on Computer-Aided Design*, New York, NY, 2024, pp. 1–9.
- [32] Z. Wang, Z. Geng, Z. Tu, J. Wang, Y. Qian, Z. Xu, Z. Liu, S. Xu, Z. Tang, S. Kai *et al.*, “Benchmarking end-to-end performance of AI-based chip placement algorithms,” *arXiv preprint*, 2024.
- [33] L. Wei, W.-C. Oon, W. Zhu, and A. Lim, “A skyline heuristic for the 2D rectangular packing and strip packing problems,” *European Journal of Operational Research*, vol. 215, no. 2, pp. 337–346, 2011.
- [34] C. Wolf, J. Glaser, and J. Kepler, “Yosys,” <https://github.com/YosysHQ/yosys>.
- [35] K. Xue, R.-T. Chen, X. Lin, Y. Shi, S. Kai, S. Xu, and C. Qian, “Reinforcement learning policy as macro regulator rather than macro placer,” in *Advances in Neural Information Processing Systems*, Vancouver, Canada, 2024, pp. 140 565–140 588.
- [36] X. Zhao, T. Wang, R. Jiao, and X. Guo, “Standard cells do matter: Uncovering hidden connections for high-quality macro placement,” in *Proceedings of Design, Automation & Test in Europe Conference*, Valencia, Spain, 2024, pp. 1–6.
- [37] Y. Zhao, L. Zou, and B. Yu, “Physical design for advanced 3D ICs: Challenges and solutions,” in *Proceedings of the International Symposium on Physical Design*, Austin, TX, 2025, in press.
- [38] Y. Zhao, P. Liao, S. Liu, J. Jiang, Y. Lin, and B. Yu, “Analytical heterogeneous die-to-die 3-D placement with macros,” *IEEE Transactions on Computer-Aided Design of Integrated Circuits and Systems*, vol. 44, no. 2, pp. 402–415, 2025.
- [39] Z.-H. Zhou, Y. Yu, and C. Qian, *Evolutionary Learning: Advances in Theories and Algorithms*. Springer, 2019.
- [40] L. Zhu, L. Bamberg, S. S. K. Pentapati, K. Chang, F. Catthoor, D. Milojevic, M. Komalan, B. Cline, S. Sinha, X. Xu, A. Garcia-Ortiz, and S. K. Lim, “High-performance logic-on-memory monolithic 3-D IC designs for Arm Cortex-A processors,” *IEEE Transactions on Very Large Scale Integration (VLSI) Systems*, vol. 29, no. 6, pp. 1152–1163, 2021.